nature nanotechnology

LETTERS

PUBLISHED ONLINE: 17 NOVEMBER 2013 | DOI: 10.1038/NNANO.2013.229

Engineering myosins for long-range transport on actin filaments

Tony D. Schindler[1†], Lu Chen[1], Paul Lebel[1,2], Muneaki Nakamura[1,3] and Zev Bryant[1,4*]

Cytoskeletal motors act as cargo transporters in cells[1] and may be harnessed for directed transport applications in molecular detection and diagnostic devices[2]. High processivity, the ability to take many steps along a track before dissociating[3], is often a desirable characteristic because it allows nanoscale motors to transport cargoes over distances on the scale of micrometres, *in vivo* and *in vitro*. Natural processive myosins[4,5] are dimeric and use internal tension to coordinate the detachment cycles of the two heads[6–8]. Here, we show that processivity can be enhanced in engineered myosins using two non-natural strategies designed to optimize the effectiveness of random, uncoordinated stepping: (1) the formation of three-headed and four-headed myosins and (2) the introduction of flexible elements between heads. We quantify improvements using systematic single-molecule characterization of a panel of engineered motors. To test the modularity of our approach, we design a controllably bidirectional myosin that is robustly processive in both forward and backward directions, and also produce the fastest processive cytoskeletal motor measured so far, reaching a speed of 10 μm s^{-1}.

Previous investigations have shown that processive myosin motion can be tolerant to dramatic changes in lever arm structure and mechanics[9,10]. These studies challenged the idea that processivity depends critically on head–head coordination mediated by internal strain. Indeed, although natural dimeric motors such as myosin V and myosin VI make use of strain-dependent gating of nucleotide exchange to prevent unproductive detachment of the front head[6–8], this mechanism may yield only modest gains in processivity relative to uncoordinated stepping[10]. Processivity without coordination has also been observed and discussed in recent studies of cytoplasmic dynein[11,12]. Processive motion of a dimeric motor can be explained by the statistics of independently cycling monomers, which are dependent on the kinetic properties of the catalytic head. Specifically, the motor variant must have a high duty ratio, defined as the fraction of the mechanochemical cycle spent bound to the filament[3].

Models of uncoordinated stepping suggest that trimeric or tetrameric myosins, which have not been observed in nature, could be dramatically more processive than dimers. Potential gains are illustrated by a toy kinetic model, which has been useful for conceptual discussions of processivity[7,10], in which the mechanochemical pathway of a myosin head is approximated by a two-state cycle governed by an attachment rate k_{on} and a detachment rate k_{off}. With three or four heads and a high duty ratio $r = k_{on}/(k_{on} + k_{off})$, the termination of a run by simultaneous detachment of all heads becomes an unlikely event (see Supplementary section 'Modelling'). This simple picture ignores the potentially detrimental effects of additional heads, which could include disruption of natural strain-mediated nucleotide gating, unintentional introduction of unproductive gating, or interference with actin rebinding due to mechanical interactions between heads or due to site occlusion.

To test whether increasing the number of heads can improve the processivity of engineered motors, we designed a series of constructs based on myosin VI. Myosin VI has a high duty ratio[5] of 0.85–0.95 (refs 10,13) and is processive in dimeric constructs[5,10], including chimeric dimers with artificial lever arms composed of two spectrin repeats[9,10]. We created $M6DI_{816}2R{\sim}DIM$, $M6DI_{816}2R{\sim}TRI$ and $M6DI_{816}2R{\sim}TET$ by fusing the chimeric myosin VI motor to engineered coiled coil variants[14] GCN4-pIL, GCN4-pII and GCN4-pLI (DIM, TRI and TET) to generate dimeric, trimeric and tetrameric motors, respectively (Fig. 1; Supplementary Fig. 5). We used single-fluorophore tracking (Supplementary Movies 1,2) to quantify the processivities of the engineered constructs. For all ATP concentrations investigated, motor trajectories (Fig. 1a) show run lengths that increase steeply with increasing oligomerization state (Fig. 1b). $M6DI_{816}2R{\sim}TRI$ and $M6DI_{816}2R{\sim}TET$ suffer only minor reductions in velocity relative to their dimeric counterpart (Fig. 1c).

To further characterize the behaviour of the $M6DI_{816}2R$ constructs, we analysed motor trajectories at high resolution using evanescent dark-field gold nanoparticle tracking[15]. Individual steps were observable in $M6DI_{816}2R{\sim}DIM$, TRI and TET trajectories (Fig. 1d). Step size distributions depend on the oligomerization state (Fig. 1e); trimers and tetramers show increased frequencies of backsteps and short steps relative to dimers. Overall, trimers and tetramers have slightly shorter mean displacements per step, but many more steps per diffusive encounter.

Shortening the lever arms of our dimers, trimers and tetramers results in substantially reduced run lengths. $M6DI_{816}1R{\sim}DIM$, $M6DI_{816}1R{\sim}TRI$ and $M6DI_{816}1R{\sim}TET$ (Fig. 2) were generated by truncating the lever arms of the $M6DI_{816}2R$ constructs to only one spectrin repeat (1R). Only $M6DI_{816}1R{\sim}TET$ yields measurably processive runs, and these runs are observable only at low [ATP] (Fig. 2, Table 1). Engineered myosins with shortened lever arms have displayed low processivities in a number of previous studies[16,17], including our work on controllable bidirectional myosins[18]. Possible causes include inhibition of rebinding due to increased strain in 2-head-bound states[16,17,19], aberrant gating due to high and/or off-axis strain, and inaccessibility of preferred off-axis sites due to surface-bound filaments.

To address possible causes of reduced processivity, we created modified $M6DI_{816}1R$ constructs in which we added a 'slack' element consisting of a spectrin repeat flanked with flexible $(Gly\text{-}Ser\text{-}Gly)_4$ linkers on both sides (Fig. 2). Without extending the rigid lever arm, this slack element is expected to provide increased

[1]Department of Bioengineering, Stanford University, Stanford, California 94305, USA, [2]Department of Applied Physics, Stanford University, Stanford, California 94305, USA, [3]Department of Chemistry, Stanford University, Stanford, California 94305, USA, [4]Department of Structural Biology, Stanford University School of Medicine, Stanford, California 94305, USA, [†]Present address: DuPont Industrial Biosciences, Cedar Rapids, Iowa 52404, USA.
*e-mail: zevry@stanford.edu

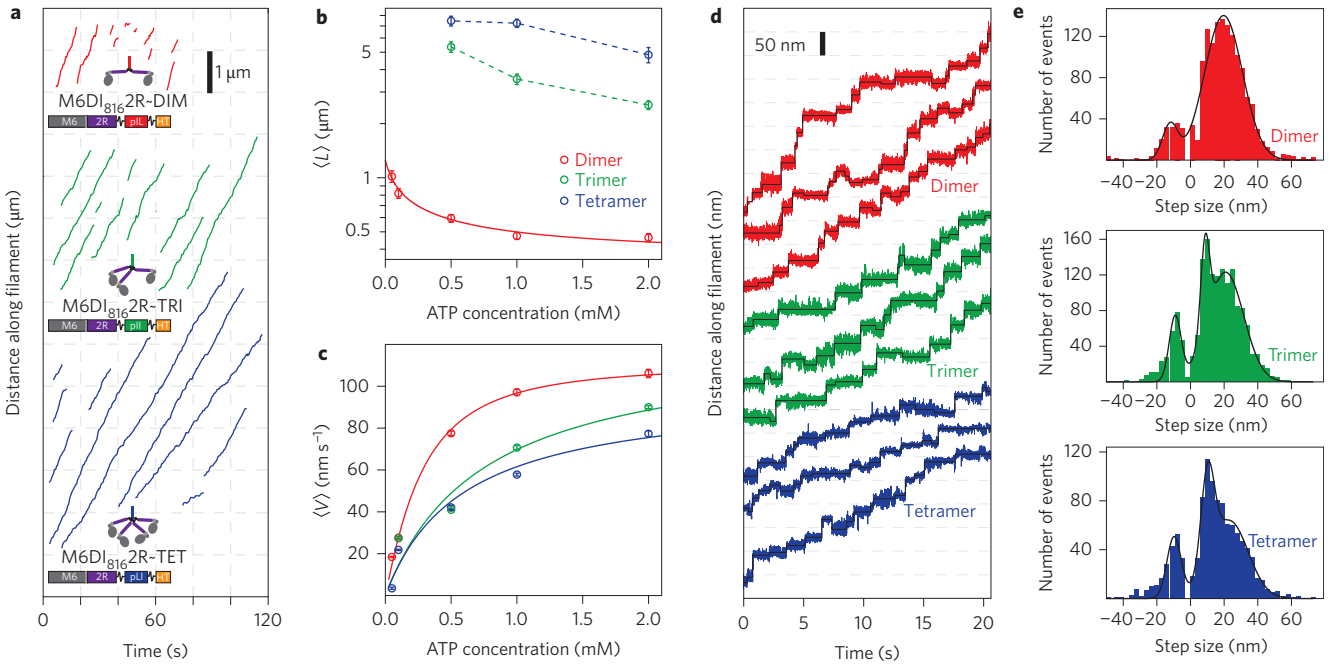

Figure 1 | Multimerization effects on engineered myosin VI processivity and stepping behaviour. a, Single-molecule fluorescence trajectories for M6DI$_{816}$2R dimers (red), trimers (green) and tetramers (blue) recorded at 2 mM ATP together with corresponding cartoons and block diagrams, showing differences due to the oligomerization state. **b**, Mean run lengths as a function of [ATP]. M6DI$_{816}$2R~DIM is fit to a three-state model[10], yielding $k_{rebind} = 290 \pm 30\ s^{-1}$, $k_{off}^{ADP} = 5.8 \pm 0.1\ s^{-1}$, $k_{on}^{ATP} = 0.015 \pm 0.001\ s^{-1}\ \mu M^{-1}$, and the defect parameter $d = 63 \pm 6$ steps. **c**, Motor velocities. M6DI$_{816}$2R~DIM is fit to the three-state model, and M6DI$_{816}$2R~TRI and M6DI$_{816}$2R~TET are fit to Michaelis-Menten kinetics. Trimer, $K_M = 740 \pm 40\ \mu M$ and $V_{max} = 120 \pm 2\ nm\ s^{-1}$; tetramer, $K_M = 630 \pm 50\ \mu M$ and $V_{max} = 99 \pm 3\ nm\ s^{-1}$. Data are displayed as mean ± s.e.m. **d**, Gold nanoparticle tracking motor stepping traces. Raw trajectories (coloured traces, collected at 500 Hz), shown together with fits (black) generated by an automatic step-finding procedure (see Methods). **e**, Step size distributions: histograms of displacements generated by step-finding ($N > 1{,}000$ steps for each construct) are shown together with fits (black) to sums of multiple Gaussian distributions. Peak locations: dimer, −12.1 ± 0.1 nm and 19.7 ± 0.3 nm; trimer, −9.1 ± 0.1 nm, 8.7 ± 0.1 nm and 20.8 ± 0.3 nm; tetramer, −9.8 ± 0.1 nm, 10.2 ± 0.1 nm and 23.1 ± 0.3 nm. Mean displacements per step: dimer, 17.5 ± 0.4 nm; trimer, 14.4 ± 0.4 nm; tetramer, 13.2 ± 0.5 nm.

conformational freedom, reduce internal strain, and provide easier access to potential binding sites. The additional compliance should abrogate strain-mediated gating, which could reduce processivity if gating is beneficial but may increase processivity if unproductive gating is present. The addition of slack results in dramatic run length increases relative to the original M6DI$_{816}$1R constructs (Fig. 2, Table 1). M6DI$_{816}$1R~1R~TET exhibits a mean run length of $\langle L \rangle = 6.87 \pm 0.80\ \mu m$ (mean ± s.e.m.) at 2 mM ATP. In comparison, M6DI$_{816}$1R~TET is not processive at 2 mM ATP, and has a mean run length of only $\langle L \rangle = 0.24 \pm 0.02\ \mu m$ at 50 μM ATP.

We created additional constructs to verify that the beneficial effect of additional compliance does not depend on having more total spectrin repeats in the motor. M6DI$_{816}$~1R~TRI and M6DI$_{816}$~1R~TET (Fig. 2, Table 1) differ from M6DI$_{816}$1R~TRI and M6DI$_{816}$1R~TET only in the insertion of a (Gly-Ser-Gly)$_4$ linker (~) between the motor domain and lever arm. Both constructs have much longer mean run lengths than their M6DI$_{816}$1R counterparts (Fig. 2, Table 1) (Supplementary Movie 3).

We tested the generalizability of our multimerization and slack strategies by constructing engineered motors based on myosin XI, a class with properties that differ significantly from myosin VI. Myosins in this fast and plus-end directed class[20,21] are found in plants and algae and are responsible for transport of golgi stacks, peroxisomes and mitochondria[22], and for cytoplasmic streaming[23]. Processive motion of wild-type myosin XI dimers purified from *Nicotiana tabacum* has been recorded[21] at 7 $\mu m\ s^{-1}$, the fastest previously observed processive movement of a cytoskeletal motor. No processive behaviour has been reported for other native myosin XI complexes (such as the well-studied *Chara corallina* motor, which is reported to have a low duty ratio of ~0.34–0.49; ref. 20) or for any recombinantly produced myosin XI protein.

We created engineered myosin XI motors that lack any rigidly attached lever arms, fusing only our slack element ~1R~ and engineered coiled coil domains (DIM, TRI, TET) to the catalytic domain (CD) of myosin XI from *Nicotiana tabacum* (NM11) or *Chara corallina* (CM11). We measured processive motion for NM11CD$_{738}$~1R~DIM, TRI and TET, and CM11CD$_{746}$~1R~DIM and TET (Fig. 3a). As seen with our myosin VI constructs, processivity increased with oligomerization state (Fig. 3b). These motors move substantially faster than the myosin VI multimers (Fig. 3c; Supplementary Movie 4).

Table 1 | Effects of increased flexibility on myosin VI constructs with short lever arms.

Construct	⟨*L*⟩ (μm)
M6DI$_{816}$1R~DIM	Not measurable (*)
M6DI$_{816}$1R~1R~DIM	0.64 ± 0.05 (*)
M6DI$_{816}$1R~TRI	Not measurable
M6DI$_{816}$1R~1R~TRI	2.20 ± 0.14
M6DI$_{816}$1R~TET	Not measurable
M6DI$_{816}$1R~1R~TET	6.87 ± 0.80
M6DI$_{816}$1R~TRI	Not measurable
M6DI$_{816}$~1R~TRI	0.44 ± 0.05
M6DI$_{816}$1R~TET	0.24 ± 0.02 (*)
M6DI$_{816}$~1R~TET	7.66 ± 0.35 (*)

Mean run lengths are compared between 1R and 1R~1R (top) and between 1R and ~1R (bottom) for single-molecule trajectories (Fig. 2) acquired at 2 mM or *, 50 μM ATP. Data are shown as mean ± s.e.m.

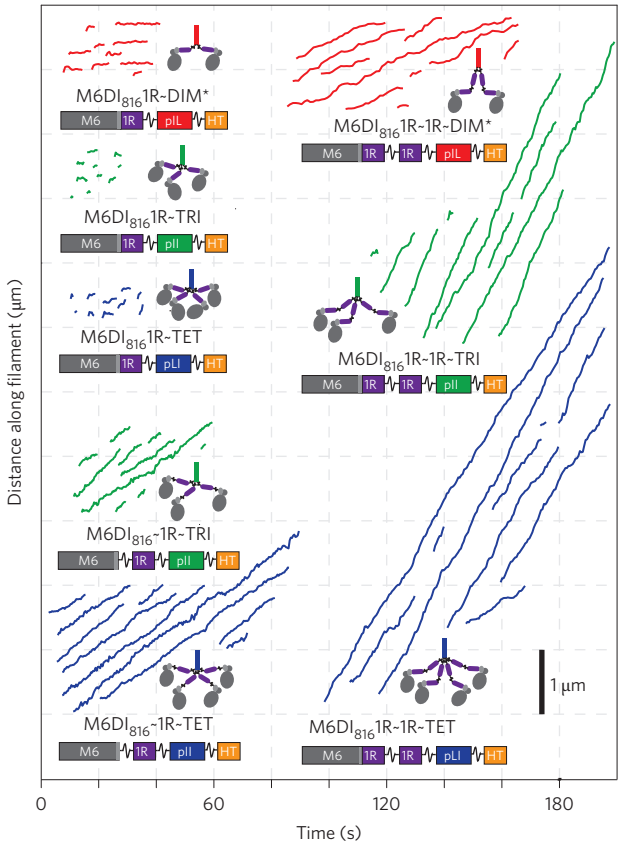

Figure 2 | Effects of increased flexibility on myosin VI constructs with short lever arms. Single-molecule fluorescence trajectories for dimers (red), trimers (green) and tetramers (blue) were recorded at 2 mM ATP or *, 50 µM, showing differences due to addition of a slack element (~1R~) or insertion of a simple flexible linker (~).

Unexpectedly, a comparison of the closely related $CM11CD_{746}$~1R~ and $NM11CD_{738}$~1R~ constructs also illuminates specialized properties of the *Chara* motor. At most ATP concentrations, $CM11CD_{746}$~1R~ constructs are both faster and more processive than their $NM11CD_{738}$~1R~ counterparts. When comparing myosin classes, there is often a trade-off between processivity and speed[24], which may be understood on the basis of simple kinetic competition (Supplementary section 'Modelling'): a short-lived actin-bound state favours high velocities, but (because detachment of the bound head competes with attachment of the free head) disfavours processivity. The simultaneous advantage in speed and processivity of *Chara* M11 over *Nicotiana* M11 may be related to the unusual charge distribution in *Chara* myosin actin binding loops[25], which has previously been proposed to enable high speed without sacrificing actin affinity.

Having developed a general approach for engineering processivity, we applied it to the design of two processive motors with two different properties desirable for potential applications: controllable bidirectionality and high speed. For both design targets, we chose to make tetramers with slack elements to achieve maximum processivity while counteracting potential detrimental effects from short lever arm lengths.

We previously engineered a chemically controlled bidirectional myosin that switches direction in response to calcium concentration[18]. MCaR-2IQ-DIM exhibits processive motion in both (+) and (−) directions. However, this construct is not measurably processive at saturating ATP, and shows only moderate run lengths even at 50 µM ATP: $\langle L \rangle = 550$ nm for (−)-end directed motion and $\langle L \rangle = 170$ nm for (+)-end directed motion. Here, we

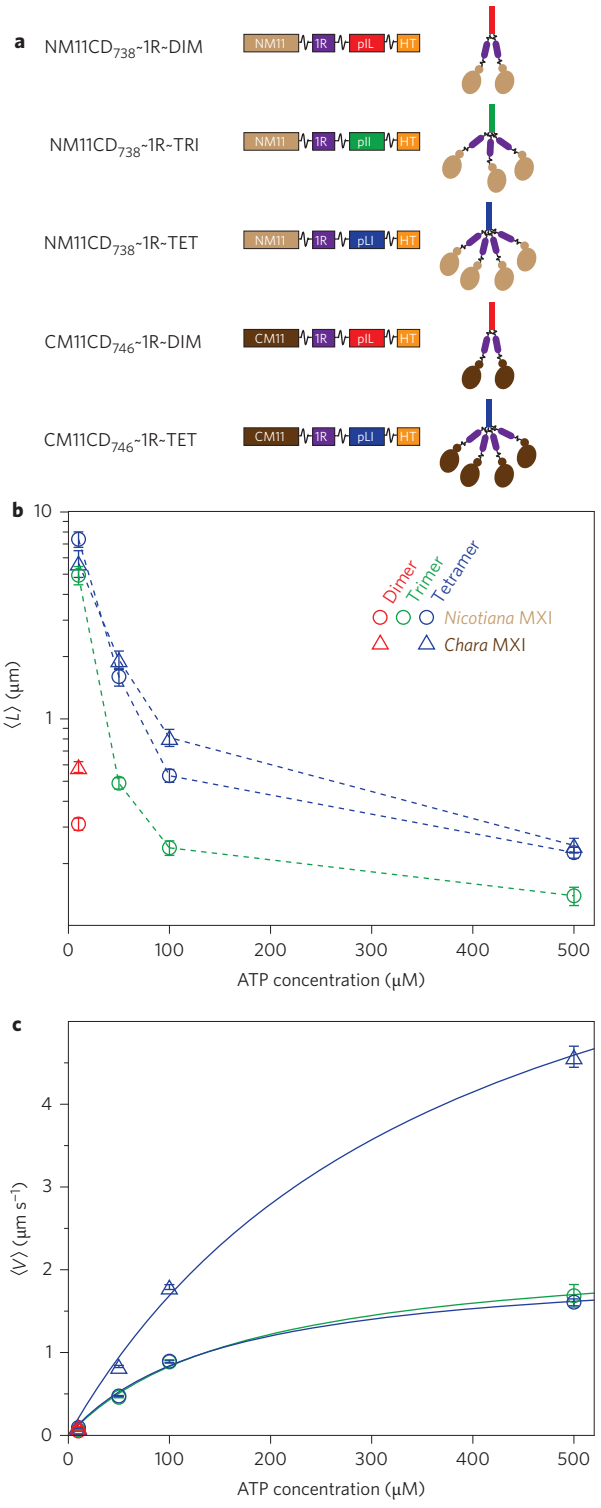

Figure 3 | Characterization of engineered myosin XI motors. a, Cartoons and block diagrams for constructs using the *N. tabacum* (light brown) and *C. corallina* myosin XI (dark brown) catalytic domains. **b**,**c**, Run lengths (**b**) and velocities (**c**) (mean±s.e.m.) as a function of [ATP].

create MCaR-2IQ~1R~TET (Fig. 4a) by fusing MCaR-2IQ to a flexible $(Gly\text{-}Ser\text{-}Gly)_4$ linker, a spectrin repeat (1R), an additional flexible linker and the tetrameric GCN4-pLI coiled coil (TET). MCaR-2IQ~1R~TET is highly processive and has mean run lengths at 2 mM ATP that exceed those of MCaR-2IQ-DIM at 50 µM ATP (Fig. 4b). High processivity facilitates new experiments

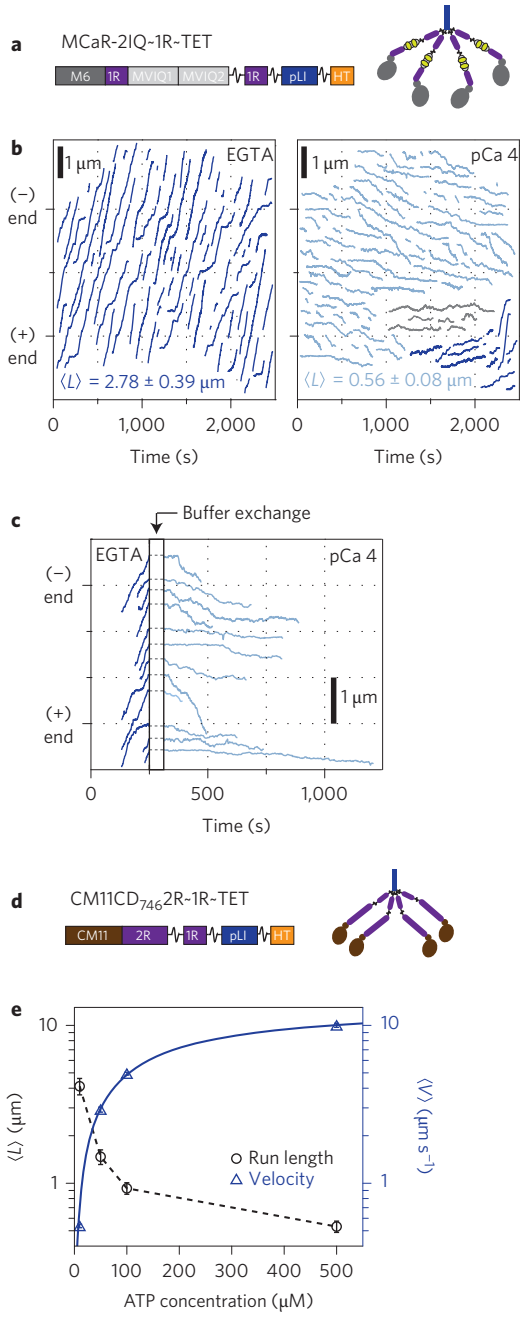

Figure 4 | Characterization of design targets for combining processivity with other desirable characteristics. a, MCaR-2IQ~1R~TET schematic. **b**, MCaR-2IQ~1R~TET is processive at 2 mM ATP in both low (EGTA) and high (pCa 4) calcium conditions. Randomly selected motor trajectories illustrate predominantly minus-end directed movement in EGTA (99.4% minus (dark blue), 0.6% plus, $N = 165$) and predominantly plus-end directed movement in pCa 4 (83.3% plus (light blue), 2.1% mixed (grey), and 14.6% minus (dark blue), $N = 96$). Minus-end directed run lengths in EGTA and plus-end directed run lengths in pCa 4 are displayed as mean ± s.e.m. Filament orientations were determined using $M6DI_{816}2R{\sim}DIM$ as a minus-end directed control[18]. Average velocities were $\langle V \rangle = 8 \pm 1$ nm s^{-1} for minus-end directed runs in EGTA and $\langle V \rangle = 1 \pm 0.1$ nm s^{-1} for plus-end directed runs in pCa 4 (mean ± s.e.m.). **c**, Dynamic switching of individual motors was accomplished using *in situ* buffer exchange. Duration of buffer exchange is approximate. **d**, Schematic of $CM11CD_{746}2R{\sim}1R{\sim}TET$. **e**, $CM11CD_{746}2R{\sim}1R{\sim}TET$ is processive over a range of [ATP], with processive velocities up to $\langle V \rangle = 10.0 \pm 0.3$ μm s^{-1}. Velocity and run length data are shown as mean ± s.e.m.

in which individual motors are dynamically switchable via *in situ* buffer exchange (Fig. 4c; Supplementary Movies 5A–C).

Chara corallina myosin XI is the fastest known cytoskeletal motor[26]. Our results (Fig. 3) show that *Chara* myosin can be incorporated into processive tetramers, although no processive behaviour has previously been reported. We reasoned that if we could increase the speed of our processive *Chara* constructs by adding a rigidly attached lever arm, we might achieve velocities exceeding any known processive cytoskeletal motors. Building on previous work in which the lever arm of the *Chara* myosin was successfully replaced with two spectrin repeats (2R)[27], we generated a tetrameric construct containing a 2R lever arm and a ~1R~ slack element. $CM11CD_{746}2R{\sim}1R{\sim}TET$ (Fig. 4d) remains measurably processive at velocities up to $\langle V \rangle = 10$ μm s^{-1} (Fig. 4e; Supplementary Movie 6). To our knowledge, this is the fastest processive speed measured for a cytoskeletal motor.

Previous work on multimotor cargo transport has established that dimeric processive motors have longer run lengths when assembled into teams of two or more dimers[28–32]. Using bead assemblies[29,33] or DNA scaffolds[28,30,31], this effect has been observed for kinesin-1[28,29,31,32], myosin V[30] and dynein[28,33]. Here, we have shown that engineered monomers can be assembled into processive complexes; fine-tuned coordination and native dimer architectures are disposable[9,10], and effective processivity enhancement can be achieved by forming multiheaded constructs and introducing flexible spacers designed to increase diffusive freedom and reduce internal tension. Quantitative improvements in processivity, while smaller than seen for a toy model that ignores interference effects and other details (Supplementary Fig. 3), are larger than has generally been reported for comparable multimotor assemblies. For both $M6DI_{816}2R$ and $CM11CD_{746}$ constructs, the tetramer is approximately ten times more processive than the dimer, which may be compared with an approximately twofold improvement in processivity when coupling two myosin V dimers together using a DNA scaffold[30]. Our measurements complement the recent discovery of processive motion in small defined assemblies of kinesin-14 dimers, which are non-processive in isolation[32].

This work provides a general approach for increasing the processivities of engineered myosins in synthetic biology or nanotechnology applications. The modularity of the approach allows high processivity to be combined with complex engineered properties such as directionality control, or with higher velocities than are normally associated with processive motors. Engineered complexes are simply and efficiently assembled (Supplementary Fig. 5) upon expression of a single polypeptide chain, and should be deployable *in vivo* for modifying the parameters of cargo transport processes[34]. Engineered motors may also be used for *in vitro* imitations of these cellular systems, which achieve effective long-range transport through a combination of processive stepping, high filament densities (to favour rebinding after dissociation) and high motor velocities[35]. In diagnostic device designs that use molecular motors to overcome diffusion limits for sensitive detection[36] or perform molecular sorting tasks[37], long-range transport has often been implemented using filament-based cargo carriers[2]. New processive motors will enhance the capabilities of alternative designs using motor-based cargo carriers[38], allowing for further miniaturization and molecular customization and control.

Methods

Proteins. DNA constructs were assembled from modules encoding porcine myosin VI (residues 1–816), *Chara corallina* myosin XI (residues 1–746), *Nicotiana tabacum* myosin XI (residues 1–738), *Dictyostelium* α-actinin (residues 266–388 for 1R and residues 266–502 for 2R) and engineered GCN4 leucine zipper variants pIL, pII and pLI[14] (Supplementary Fig. 4). All constructs contained a C-terminal flexible linker, HaloTag protein sequence (Promega) and flag tag (DYKDDDDK), and were cloned into pBiEx-1 (Novagen). Proteins were expressed via direct transfection

of SF9 cells and purified and labelled with TMR HaloTag ligand (Promega) or PEG–biotin HaloTag ligand (Promega) as previously described[9,10].

Single-molecule fluorescence tracking assays. Assays were carried out in Assay Buffer (AB) containing 25 mM imidazole, 25 mM KCl, 1 mM EGTA and $MgCl_2$. The concentration of $MgCl_2$ added varied depending on the final assay ATP concentration to give 2 mM free Mg^{2+}, according to MAXCHELATOR (http://maxchelator.stanford.edu). Calmodulin (4 μM) was added when assaying myosin VI constructs. Blocking buffer consisted of AB with 1 mg ml^{-1} BSA (Sigma). Imaging buffer consisted of AB with the desired ATP concentration, 1 mM phosphocreatine, 100 μg ml^{-1} creatine phosphokinase, 0.4% glucose, 0.2 mg ml^{-1} glucose oxidase, 36 μg ml^{-1} catalase and 1.8 mM trolox. MCaR-2IQ∼1R∼TET constructs were assayed in buffers with 2 μM calmodulin and either pCa 4 or EGTA as described[18], with $MgCl_2$ added to yield 2 mM free Mg^{2+} upon addition of 2 mM ATP in imaging buffer. Assays were performed essentially as described[10], except that plasma-cleaned coverslips were used without any nitrocellulose coating. Briefly, *N*-ethyl maleimide-inactivated full-length skeletal muscle myosin (a gift from R. Cooke) was used to immobilize actin filaments stabilized with excess Alexa 633 phalloidin (Invitrogen). Nonspecific binding was minimized by incubation with blocking buffer. Motors were added in imaging buffer. Videomicroscopy data were collected on an electron-multiplying charge-coupled device camera (Andor) under objective-side total-internal-reflection fluorescence excitation using a 532 nm diode-pumped solid-state laser (Coherent) through a 1.49 NA ×100 objective (Nikon). Actin filaments were imaged before recording assay videos with a separate emission filter set. Motor trajectories were tracked using custom software as described[10]. To avoid artefacts due to undersampling of short runs[10], an analysis cutoff was used: only trajectories lasting at least three frames and travelling more than two pixels (216 nm) were scored for velocity, run length and directionality. For the high-velocity motor $CM11CD_{746}$2R∼1R∼TET assayed at 100 μM and 500 μM ATP, the cutoff was increased to three pixels (324 nm) (Supplementary Table 2). Mean run lengths were corrected for runs that terminated at the end of a filament using the Kaplan–Meier survivor function, and the reported errors of the mean (s.e.m.) are the error estimates from this function (Supplementary Fig. 6). Constructs with mean run lengths $\langle L \rangle$ greater than two s.e.m. above one pixel (108 nm) were deemed 'measurably processive'. 'Mixed' runs for MCaR-2IQ∼1R∼TET were defined as runs that showed >216 nm movement in one direction and subsequently >216 nm in the other direction. Velocity error estimates were calculated as described[10], except that s.e.m. weighting was not used and the number of sets used in bootstrapping was equal to the number of runs scored. Fit error estimates for model fit parameters were calculated as described[10]. A summary of run length and velocity data is provided in Supplementary Table 1.

Gold nanoparticle tracking assays. NeutrAvidin-coated 50 nm gold nanospheres (Nanopartz) were washed into binding buffer (500 mM NaCl, 40 mM Tris pH 7.5, 0.2% (vol/vol) tween-20 (Sigma) and 1 mg ml^{-1} BSA) by centrifugation and resuspension. PEG–biotin labelled proteins were incubated with washed beads for 15 min at 25 °C before dilution into imaging buffer. Assays were carried out as for the single-molecule fluorescence tracking assays, with the addition of 0.2% (vol/vol) tween-20 in the blocking buffer and 1 mg ml^{-1} BSA and 0.2% tween-20 (vol/vol) in the imaging buffer, which contained 50 μM ATP. Gold particles were imaged using objective-side evanescent dark-field microscopy. Laser illumination was provided by a 532 nm diode-pumped solid-state laser (Spectra-Physics) through a 1.49 NA ×60 objective (Nikon) and totally internally reflected at the sample interface; additional details of the microscope design will be presented elsewhere (Lebel *et al.*, submitted). Scattered light was imaged on a high-speed CMOS camera (Mikrotron Ecosens CL) at 500 Hz. Analysis details are provided in the Supplementary Methods.

Received 16 January 2013; accepted 8 October 2013; published online 17 November 2013

References

1. Vale, R. D. The molecular motor toolbox for intracellular transport. *Cell* **112,** 467–480 (2003).
2. Korten, T., Månsson, A. & Diez, S. Towards the application of cytoskeletal motor proteins in molecular detection and diagnostic devices. *Curr. Opin. Biotechnol.* **21,** 477–488 (2010).
3. Howard, J. Molecular motors: structural adaptations to cellular functions. *Nature* **389,** 561–567 (1997).
4. Mehta, A. D. *et al.* Myosin-V is a processive actin-based motor. *Nature* **400,** 590–593 (1999).
5. Rock, R. S. *et al.* Myosin VI is a processive motor with a large step size. *Proc. Natl Acad. Sci. USA* **98,** 13655–13659 (2001).
6. Rosenfeld, S. S. & Sweeney, H. L. A model of myosin V processivity. *J. Biol. Chem.* **279,** 40100–40111 (2004).
7. Veigel, C., Wang, F., Bartoo, M. L., Sellers, J. R. & Molloy, J. E. The gated gait of the processive molecular motor, myosin V. *Nature Cell Biol.* **4,** 59–65 (2001).
8. Robblee, J. P., Olivares, A. O. & de la Cruz, E. M. Mechanism of nucleotide binding to actomyosin VI: evidence for allosteric head-head communication. *J. Biol. Chem.* **279,** 38608–38617 (2004).
9. Liao, J-C., Elting, M. W., Delp, S. L., Spudich, J. A. & Bryant, Z. Engineered myosin VI motors reveal minimal structural determinants of directionality and processivity. *J. Mol. Biol.* **392,** 862–867 (2009).
10. Elting, M. W., Bryant, Z., Liao, J-C. & Spudich, J. A. Detailed tuning of structure and intramolecular communication are dispensable for processive motion of myosin VI. *Biophys. J.* **100,** 430–439 (2011).
11. Qiu, W. *et al.* Dynein achieves processive motion using both stochastic and coordinated stepping. *Nature Struct. Mol. Biol.* **19,** 193–200 (2012).
12. DeWitt, M. A., Chang, A. Y., Combs, P. A. & Yildiz, A. Cytoplasmic dynein moves through uncoordinated stepping of the AAA+ ring domains. *Science* **335,** 221–225 (2012).
13. De La Cruz, E. M. Kinetic mechanism and regulation of myosin VI. *J. Biol. Chem.* **276,** 32373–32381 (2001).
14. Harbury, P. B., Zhang, T., Kim, P. S. & Alber, T. A switch between two-, three-, and four-stranded coiled coils in GCN4 leucine zipper mutants. *Science* **262,** 1401–1407 (1993).
15. Dunn, A. R., Chuan, P., Bryant, Z. & Spudich, J. A. Contribution of the myosin VI tail domain to processive stepping and intramolecular tension sensing. *Proc. Natl Acad. Sci. USA* **107,** 7746–7750 (2010).
16. Sakamoto, T. *et al.* Neck length and processivity of myosin V. *J. Biol. Chem.* **278,** 29201–29207 (2003).
17. Purcell, T. J., Morris, C., Spudich, J. A. & Sweeney, H. L. Role of the lever arm in the processive stepping of myosin V. *Proc. Natl Acad. Sci. USA* **99,** 14159–14164 (2002).
18. Chen, L., Nakamura, M., Schindler, T. D., Parker, D. & Bryant, Z. Engineering controllable bidirectional molecular motors based on myosin. *Nature Nanotech.* **7,** 252–256 (2012).
19. Sakamoto, T., Yildez, A., Selvin, P. R. & Sellers, J. R. Step-size is determined by neck length in myosin V. *Biochemistry* **44,** 16203–16210 (2005).
20. Sumiyoshi, H., Ooguchi, M., Ooi, A., Okagaki, T. & Higashi-Fujime, S. Insight into the mechanism of fast movement of myosin from *Chara corallina*. *Cell Motil. Cytoskel.* **64,** 131–142 (2007).
21. Tominaga, M. *et al.* Higher plant myosin XI moves processively on actin with 35 nm steps at high velocity. *EMBO J.* **22,** 1263–1272 (2003).
22. Prokhnevsky, A. I., Peremyslov, V. V. & Dolja, V. V. Overlapping functions of the four class XI myosins in Arabidopsis growth, root hair elongation, and organelle motility. *Proc. Natl Acad. Sci. USA* **105,** 19744–19749 (2008).
23. Shimmen, T. & Yokota, E. Cytoplasmic streaming in plants. *Curr. Opin. Cell Biol.* **16,** 68–72 (2004).
24. Mehta, A. Myosin learns to walk. *J. Cell Sci.* **114,** 1981–1998 (2001).
25. Ito, K., Yamaguchi, Y., Yanase, K., Ichikawa, Y. & Yamamoto, K. Unique charge distribution in surface loops confers high velocity on the fast motor protein Chara myosin. *Proc. Natl Acad. Sci. USA* **106,** 21585–21590 (2009).
26. Ito, K. *et al.* Kinetic mechanism of the fastest motor protein, Chara myosin. *J. Biol. Chem.* **282,** 19534–19545 (2007).
27. Ito, K. *et al.* Recombinant motor domain constructs of *Chara corallina* myosin display fast motility and high ATPase activity. *Biochem. Biophys. Res. Commun.* **312,** 958–964 (2003).
28. Derr, N. D. *et al.* Tug-of-war in motor protein ensembles revealed with a programmable DNA origami scaffold. *Science* **338,** 662–665 (2012).
29. Beeg, J. *et al.* Transport of beads by several kinesin motors. *Biophys. J.* **94,** 532–541 (2008).
30. Lu, H. *et al.* Collective dynamics of elastically coupled myosin V motors. *J. Biol. Chem.* **287,** 27753–27761 (2012).
31. Rogers, A. R., Driver, J. W., Constantinou, P. E., Kenneth Jamison, D. & Diehl, M. R. Negative interference dominates collective transport of kinesin motors in the absence of load. *Phys. Chem. Chem. Phys.* **11,** 4882–4889 (2009).
32. Furuta, K. *et al.* Measuring collective transport by defined numbers of processive and nonprocessive kinesin motors. *Proc. Natl Acad. Sci. USA* **110,** 501–506 (2013).
33. Mallik, R., Petrov, D., Lex, S. A., King, S. J. & Gross, S. P. Building complexity: an *in vitro* study of cytoplasmic dynein with *in vivo* implications. *Curr. Biol.* **15,** 2075–2085 (2005).
34. Goodman, B. S., Derr, N. D. & Reck-Peterson, S. L. Engineered, harnessed, and hijacked: synthetic uses for cytoskeletal systems. *Trends Cell Biol.* **22,** 644–652 (2012).
35. Smith, D. A. & Simmons, R. M. Models of motor-assisted transport of intracellular particles. *Biophys. J.* **80,** 45–68 (2001).
36. Katira, P. & Hess, H. Two-stage capture employing active transport enables sensitive and fast biosensors. *Nano Lett.* **10,** 567–572 (2010).
37. van den Heuvel, M. G. L., de Graaff, M. P. & Dekker, C. Molecular sorting by electrical steering of microtubules in kinesin-coated channels. *Science* **312,** 910–914 (2006).
38. Amrute-Nayak, M. *et al.* Targeted optimization of a protein nanomachine for operation in biohybrid devices. *Angew. Chem. Int. Ed.* **49,** 312–316 (2010).

Acknowledgements

The authors thank M.W. Elting and K. Aathavan for valuable insights and discussions, R. Cooke for providing full-length skeletal muscle myosin, S. Sutton for providing purified actin, and A.J. Lam for native PAGE advice and assistance. This work was supported by a Pew Scholars Award and a National Institutes of Health (NIH) grant (DP2 OD004690 to Z.B.). T.D.S. was supported by a Stanford Graduate Fellowship, a Ruth L. Kirschstein NRSA Graduate Training Program in Biotechnology (NIH grant 5T32GM008412 awarded to Stanford University) and a Siebel Scholars award. P.L. was supported by a Stanford Interdisciplinary Graduate Fellowship (SIGF) and the Natural Sciences and Engineering Research Council of Canada (award NSERC PGS-D3).

Author contributions

T.D.S. and Z.B. designed the myosin constructs. T.D.S. and L.C. performed experiments on the bidirectional design target. T.D.S. and P.L. performed gold nanoparticle tracking experiments. T.D.S. performed all other experiments with assistance from M.N. and L.C., and analysed the experimental data. Z.B. conceived and supervised the project. T.D.S. and Z.B. wrote the paper. All authors discussed the results and commented on the manuscript.

Additional information

Supplementary information is available in the online version of the paper. Reprints and permissions information is available online at www.nature.com/reprints. Correspondence and requests for materials should be addressed to Z.B.

Competing financial interests

The authors declare no competing financial interests.